A&A, 692, A78 (2024)
https://doi.org/10.1051/0004-6361/202451688

Astronomy & Astrophysics

Effects of ultrafast outflows on X-ray time lags in active galactic nuclei

Yerong Xu[1,2,3,⋆], Ciro Pinto[1], Erin Kara[4], Stefano Bianchi[5], William Alston[6], and Francesco Tombesi[7,8,9]

[1] INAF - IASF Palermo, Via U. La Malfa 153, I-90146 Palermo, Italy
[2] Università degli Studi di Palermo, Dipartimento di Fisica e Chimica, via Archirafi 36, I-90123 Palermo, Italy
[3] Department of Astronomy & Physics, Saint Mary's University, 923 Robie Street, Halifax, NS B3H 3C3, Canada
[4] MIT Kavli Institute for Astrophysics and Space Research, Massachusetts Institute of Technology, Cambridge, MA 02139, USA
[5] Dipartimento di Matematica e Fisica, Università degli Studi Roma Tre, via della Vasca Navale 84, I-00146 Roma, Italy
[6] Centre for Astrophysics Research, University of Hertfordshire, College Lane, Hatfield AL10 9AB, UK
[7] Department of Physics, University of Rome Tor Vergata, Via della Ricerca Scientifica 1, I-00133 Rome, Italy
[8] INAF - Astronomical Observatory of Rome, Via Frascati 33, 00040 Monte Porzio Catone, Italy
[9] INFN - Rome Tor Vergata, Via della Ricerca Scientifica 1, 00133 Rome, Italy

Received 29 July 2024 / Accepted 5 November 2024

ABSTRACT

Context. The time lag between soft (e.g., 0.3–1 keV) and hard (e.g., 1–4 keV) X-ray photons has been observed in many active galactic nuclei (AGNs) and can reveal the accretion process and geometry around supermassive black holes. High-frequency Fe K and soft lags are considered to originate from the light-travel distances between the corona and the accretion disk, while the propagation of the inward mass accretion fluctuation usually explains the low-frequency hard lags. Ultrafast outflows (UFOs) with a velocity range of ∼0.03 to 0.3c have also been discovered in numerous AGNs and are believed to be launched from the inner accretion disk. However, it remains unclear whether UFOs can affect the X-ray time lags.
Aims. As a pilot work, we aim to investigate the potential influence of UFOs on X-ray time lags of AGNs in a small sample.
Methods. By performing the UFO-resolved Fourier spectral timing analysis of archival *XMM-Newton* observations of three AGNs with transient UFOs – PG 1448+273, IRAS 13224-3809, and PG 1211+143 – we compare the X-ray timing products, such as lag-frequency and lag-energy spectra, of observations with and without UFO obscuration.
Results. Our results find that in each AGN, low-frequency hard lags become weak or even disappear when they are accompanied by UFOs. This change is confirmed by Monte Carlo simulations at a confidence level of at least 2.7σ. In the high-frequency domain, soft lags remain unchanged, while the Fe K reverberation lags tentatively disappear. The comparison between timing products of low- and high-flux observations on another three AGNs without UFOs (Ark 564, NGC 7469, and Mrk 335) suggests that the disappearance of low-frequency hard lags is likely related to the emergence of UFOs, not necessarily related to the source flux.
Conclusions. The presence of UFOs can affect X-ray time lags of AGNs by suppressing the low-frequency hard lags, which can be explained by an additional time delay introduced by UFOs or disk accretion energy, which should transferred to heat the corona, carried away by UFOs.

Key words. accretion, accretion disks – black hole physics – quasars: supermassive black holes – galaxies: Seyfert

1. Introduction

Many supermassive black holes (SMBHs) in the center of active galactic nuclei (AGNs) accrete materials through a geometrically thin and optically thick disk (Shakura & Sunyaev 1973). The X-ray spectra of unobscured AGNs have three primary broadband components: a power-law-like continuum originating from the inverse Compton scattering of thermal (UV) disk photons in the central hot plasma ('hot corona', Sunyaev & Titarchuk 1980; Haardt & Maraschi 1993), a reflection component from the X-ray reprocessing of coronal emission in the accretion disk (Fabian et al. 1989; George & Fabian 1991; García & Kallman 2010) including a wealth of fluorescent lines (in particular a Fe K line at ∼6.4 keV, George & Fabian 1991; Ross & Fabian 2005) and a Compton hump (>10 keV), and a blackbody-shape-like soft excess whose nature is still under debate, probably originating from a warm Comptonization (e.g., Done et al. 2012; Petrucci et al. 2018, 2020; Ballantyne et al. 2024) or relativistically blurred reflection (e.g., García et al. 2019; Xu et al. 2021), or the combination of two scenarios (Porquet et al. 2018, 2021; Xiang et al. 2022).

X-ray variability studies of unobscured AGNs have shown that the 0.3–1 keV band (referred to as the soft band), dominated by soft excess, and the Fe K band (5–7 keV), dominated by reflection, lag behind the continuum-dominated 1–4 keV band (referred to as the hard band) in the high-frequency domain (e.g., De Marco et al. 2013; Uttley et al. 2014; Kara et al. 2016). Despite the complicated soft excess origin (perhaps due to the reflection), the Fe K lag explicitly suggests light-travel distances between the corona and the accretion disk at a few gravitational radii, called X-ray reverberation lags (e.g., Fabian et al. 2009; Zoghbi et al. 2010; Kara et al. 2016). On the other hand, the low-frequency variability of unobscured AGNs commonly shows that the hard X-rays lag behind the soft emission with a time delay increasing steadily with energy. This low-frequency hard lag has been observed for several decades (e.g., Papadakis et al.

⋆ Corresponding author; yerong.xu@inaf.it

2001; Kara et al. 2013a,b, 2016). The timescales of the low-frequency X-ray lags are orders of magnitude longer than the viscous timescale of the inner accretion flow. The origin of this lag is still not well understood, though in the prevailing model is the multiplicative mass accretion fluctuation generated at large radii propagating inward to the inner accretion disk (Lyubarskii 1997; Kotov et al. 2001; Arévalo & Uttley 2006; Uttley & Malzac 2024). These time lags provide critical insights into the geometry and dynamics of the regions very close to the black hole, helping us to map out the configuration of the inner accretion environment.

Besides accreting a large amount of gas, AGNs can release part of the accumulated energy via the ejection of outflows (for review see Fabian 2012; Laha et al. 2021), some of which may have sufficient kinetic power ($L_{\rm kin} > 0.5{-}5\%L_{\rm Edd}$, $L_{\rm Edd}$ is the Eddington luminosity) to impact the evolution of the host galaxy and growth of SMBHs (e.g., Di Matteo et al. 2005; Hopkins & Elvis 2010). Ultrafast outflows (UFOs) are an extreme subclass of AGN winds with mildly relativistic speeds (>10 000 km/s), which are commonly discovered by strongly blueshifted absorption lines in X-ray spectra (Chartas et al. 2002, 2003, 2021; Pounds et al. 2003; Tombesi et al. 2010; Patrick et al. 2012; Gofford et al. 2013; Matzeu et al. 2023; Yamada et al. 2024; Xu et al. 2024). The ultrafast velocity suggests that UFOs are launched from the accretion disk within a few hundred gravitational radii close to the central SMBH (e.g., Tombesi et al. 2013), the same region probed by the X-ray spectral-timing analysis. Therefore, UFOs are expected to leave imprints on the X-ray variability of AGNs.

The variability study of UFOs has shown that UFOs produce characteristic positive "spikes" of enhanced variability in variance spectra, which exhibit the energy dependence of variability (Parker et al. 2017a, 2018, 2021; Igo et al. 2020; Härer et al. 2021). These features result from the UFO response to the continuum, where absorption lines from the UFO disappear as the X-ray flux rises (Parker et al. 2017b; Pinto et al. 2018), leading to a higher variability amplitude in energy bands affected by absorption than others dominated by the continuum.

The contribution of UFOs to the X-ray reverberation lags in the high-frequency domain was studied by Mizumoto et al. (2018, 2019), showing that the high-frequency Fe K lag may arise from the scattering in a highly ionized disk wind instead of the reflection onto the accretion disk. This alternative explanation could also reproduce the observed Fe K lags in 1H 0707-495 and Ark 564. However, the impact of UFOs on low-frequency hard lags in AGNs has not yet been investigated thoroughly. A transient UFO event was once observed by a large *XMM-Newton* campaign in PG 1211+143 (Pounds et al. 2016a,b), wherein Lobban et al. (2018) noticed that the low-frequency lag weakened in the presence of the UFO, which was explained by a change or disruption in the inner accretion flow before the reemergence or an additional soft lag introduced by other physical processes.

We would like to explore whether the coexistence of UFOs and weak low-frequency hard lags is common, and if so whether they are coincidental or causally related. To answer these questions, we have revisited the archival *XMM-Newton* dataset and selected two variable type 1 AGNs with transient UFOs; that is, PG 1448+273 and IRAS 13224-3809 (hereafter PG 1448 and IRAS 13224), to perform the X-ray lag analysis. The data of PG 1211+143 (hereafter PG 1211) have also been reanalyzed to reproduce the results in Lobban et al. (2018). The choice of *XMM-Newton* is because it has a higher orbit, and thus a longer orbital period (~48 h), than other X-ray satellites, enabling us to probe the long-timescale variability of AGN. The targets are required to be type 1 AGNs to avoid the influence of large-scale obscuration (i.e., torus, Krolik & Begelman 1988; Netzer 2013) on X-ray variability and have at least two *XMM-Newton* observations with net exposures of >30 ks with and without UFOs separately for comparison.

PG 1448 is a luminous ($L_{\rm bol} \sim 10^{45.24}$ erg/s, Rakshit et al. 2020), nearby ($z = 0.0645$), narrow-line Seyfert 1 (NLS1) galaxy, hosting a SMBH of $M_{\rm BH} \sim 10^7\,M_\odot$ (Vestergaard & Peterson 2006), indicating its accretion rate is close to the Eddington limit. PG 1448 was observed by *XMM-Newton* in 2017 (~75 ks net EPIC-pn exposure) at a low-flux state ($F_{2-10\,\rm keV} = 1.3\times10^{-12}$ erg/s/cm^2) with the presence of a UFO (~0.09c), measured by the simultaneous detection of blueshifted soft X-ray and Fe K absorption lines (Kosec et al. 2020; Laurenti et al. 2021). Recently, PG 1448 was observed by *NuSTAR* for 130 ks net exposure (250 ks duration) joint with *XMM-Newton* for ~60 ks net exposure. The observation was performed at a bright state ($F_{2-10\,\rm keV} = 4.8\times10^{-12}$ erg/s/cm^2), revealing strong X-ray variability with a generally featureless X-ray spectrum. Although the last 60 ks of the *NuSTAR* observation (without a simultaneous *XMM-Newton* exposure) exhibited a flux decline and the emergence of a UFO, no UFO was detected during the *XMM-Newton* observation (Reeves et al. 2023).

IRAS 13224 is a nearby ($z = 0.066$, Allen et al. 1991), variable (e.g., Ponti et al. 2012) NLS1 galaxy, hosting an SMBH of $M_{\rm BH} \sim 2\times10^6\,M_\odot$ (Zhou & Wang 2005; Alston et al. 2020). This target was extensively observed by *XMM-Newton* for a total of ~2 Ms, including a ~1.5 Ms campaign in 2016. The UFOs (~0.236c) found in both the soft and hard X-ray bands of IRAS 13224 show a strong dependence on the source flux, where the strength of the absorption decreases as the flux increases, explained by the over-ionization of plasma (Parker et al. 2017b; Pinto et al. 2018). High-frequency soft lag and low-frequency hard lag were significantly detected (e.g., Ponti et al. 2010; Kara et al. 2013c; Hancock et al. 2022), where the reverberation lag is positively correlated with luminosity, indicating a variable corona height (Alston et al. 2020).

PG 1211 is a nearby ($z = 0.0809$, Marziani et al. 1996) and variable (e.g., Ponti et al. 2012) NLS1 galaxy or quasar, hosting a black hole of $M_{\rm BH} \sim 1.5\times10^8\,M_\odot$ (Peterson et al. 2004). It is bright in both the optical and X-ray bands with an X-ray luminosity on the order of $\sim10^{44}$ erg/s ($L_{\rm bol} \sim 5\times10^{45}$ erg/s, Pounds et al. 2003). The source is an archetypal example of an AGN exhibiting a UFO in both UV (Kriss et al. 2018) and X-ray (e.g., Pounds et al. 2003, 2016a; Pounds & Reeves 2009; Danehkar et al. 2018; Reeves et al. 2018; Pounds & Nayakshin 2023) bands at velocities between ~0.066 and 0.2c. The large *XMM-Newton* campaign in 2014 (~630, ks) observed a complete UFO obscuration event from its emergence to its disappearance. The high-frequency reverberation lag and variable low-frequency hard lag were discovered from the same observations (Lobban et al. 2016, 2018).

The paper is organized as follows. Observations and data reduction used in this analysis are described in Sect. 2. Details of our Fourier analysis and results are shown in Sect. 3. Finally, we discuss the results and provide our conclusions in Sects. 4 and 5, respectively.

2. Data reduction

Basic information about the analyzed *XMM-Newton* observations of three AGNs is shown in Table 1. The observations are

Table 1. *XMM-Newton* observations of three AGNs analyzed in this work.

Source	Label	Obs. ID	Exposure (ks)	Count Rates (cts/s)
PG 1448+273	low-flux w/ UFO	0781430101	76	2.3
	high-flux w/o UFO	0890600101	58	11.3
IRAS 13224-3809	low-flux w/ UFO	0673580301, 0780561501, 0780561701	82, 127, 122	1.2, 1.7, 2.0
	high-flux w/o UFO	0780561601, 0792180401, 0792180601	124, 115, 118	4.0, 5.3, 5.2
PG 1211+143	low-flux w/ UFO	0745110201, 0745110301 (⋆), 0745110401, 0745110501	89, 75, 87, 51	3.1, 3.9, 4.6, 5.8
	high-flux w/o UFO	0745110101, 0745110601, 0745110701	78, 86, 89	4.7, 5.7, 4.4

Notes. (⋆)The source spectrum was extracted from an annulus region with an inner radius of 5 arcsec and an outer radius of 30 arcsec. The second column shows the label for stacked observations at two states. The observation IDs are shown in the third column. The corresponding net exposure time and count rate of EPIC-pn are listed in the fourth and fifth columns, respectively.

classified as those with or without UFOs according to the literature (Parker et al. 2017b; Pinto et al. 2018; Lobban et al. 2018; Reeves et al. 2023). To increase the signal-to-noise ratio (S/N), we stacked observations within the same class for our analysis.

For this analysis, we used the data from the *XMM-Newton* EPIC-pn camera because of its high effective area and fast readout (Jansen et al. 2001; Strüder et al. 2001). Data were reduced following standard threads with the *XMM-Newton* Science Analysis System (SAS v20.0.0) and calibration files available by February 2023. We reduced the EPIC-pn data using EPPROC and filtered the time intervals affected by the background solar flares, which show the count rates larger than 1 counts/sec in the 10–12 keV. This filter is higher than the regular threshold (0.5 count/sec), reducing interruptions in the extracted light curves caused by background flares, so that we can obtain a long continuous light curve to probe the low-frequency domain. We estimated the effect of the introduced background flares to be negligible by comparing results from this filter and those from the stricter filter with interpolated and Poisson-noise-added gaps. The net EPIC-pn exposure time and count rate are listed in Table 1. Meanwhile, for flares of <500 s in duration, the source light curve was cut out and interpolated between the flare gap by adding Poisson noise using the mean of neighboring points. The interpolation fraction is typically <1%. For gaps longer than 500 s, the data were treated as separate segments. The source and background regions were selected by a circular region with a radius of 30 arcsec centered on the source and offset but near it, respectively. The observation affected by the pile-up effect is marked by an asterisk in Table 1, and the corresponding source region has been replaced by an annulus with an inner radius of 5 arcsec and an outer radius of 30 arcsec. The background-subtracted light curves of AGNs were extracted by the EPICLCCORR package and shown in the top panels of Fig. A.1.

3. Results

Observations within the same class (i.e., with or without UFOs) were stacked, resulting in two stacked observations for each target, although the classification of IRAS 13224 observations is not explicit in the literature. However, given the flux-dependent UFO detection in IRAS 13224, UFOs are expected to be significantly detected in faint states and to become negligible in bright states. Therefore, the three brightest observations are classified as those without UFOs and the three faintest exposures are regarded as observations with UFOs. The presence or absence of UFOs in stacked spectra labeled by "low/high-flux w/wo UFO" are illustrated by the data-to-model ratios to the best-fit broad-band continuum model (shown in Fig. 1), also justifying our expectation for UFOs in IRAS 13224. The continuum model consists of an absorbed power law, a soft excess, and a reflection component. The unfolded stacked EPIC-pn spectra with respect to a power law with an index of $\Gamma = 2$ of each AGN are shown in the first column of Fig. 2. In PG 1448 and IRAS 13224, the difference between stacked spectra with and without UFOs comes from both the continuum shape and the UFO absorption features (>7 keV), while that difference in PG 1211 only occurs in the soft X-ray band, mainly dominated by the transient UFO.

3.1. Lag-frequency spectra

We used the package `pylag`[1] (Wilkins 2019) to compute the X-ray time-lag spectrum (e.g., Uttley et al. 2014). Briefly, we performed the Fourier transform of the light curves in two different energy bands and multiplied the transform from the soft band and the complex conjugate of that from the hard band, called the cross-spectrum. In this paper, we take the conventional 0.3–1.0 keV as the soft band and 1–4 keV as the hard band, except for the 0.7–1.5 keV and 2–10 keV bands for PG 1211 for consistency with the literature (Lobban et al. 2018). The segment lengths are typically 50 ks for PG 1448 and 70 ks for IRAS 13224 and PG 1211, respectively, so that we can probe the lowest frequencies possible. The minimum frequency is defined by the inverse of the segment length, and the maximum frequency is set by the frequency at which the power spectral density (PSD, see details in Appendix A) becomes dominated by Poisson noise. The argument of the cross-spectrum is the phase lag between the two light curves. The time lag is $\tau(f) = \phi(f)/2\pi f$, where $\phi(f)$ is the frequency-dependent phase lag. The uncertainty of the time lag depends on the coherence of two light curves (see details in Uttley et al. 2014). We binned the lag-frequency spectrum into equal logarithmic frequency bins and the number of frequency bins depends on the quality of the data (i.e., more bins for higher-quality data).

The lag-frequency spectra of the stacked observations in each AGN are shown in the second column of Fig. 2. The black and royal blue arrows separately refer to frequencies, where the PSD of the highest energy bin (in lag-energy spectra) becomes dominated by Poisson noise, for the "low/high-flux w/wo UFO" observations. All lag-frequency spectra in Fig. 2 successfully reveal the high-frequency soft reverberation lag (e.g., Fabian et al. 2009; Kara et al. 2013c, 2016; De Marco et al. 2013) and low-frequency hard continuum lag. The soft reverberation lag in IRAS 13224 is not obvious due

[1] https://github.com/wilkinsdr/pyLag

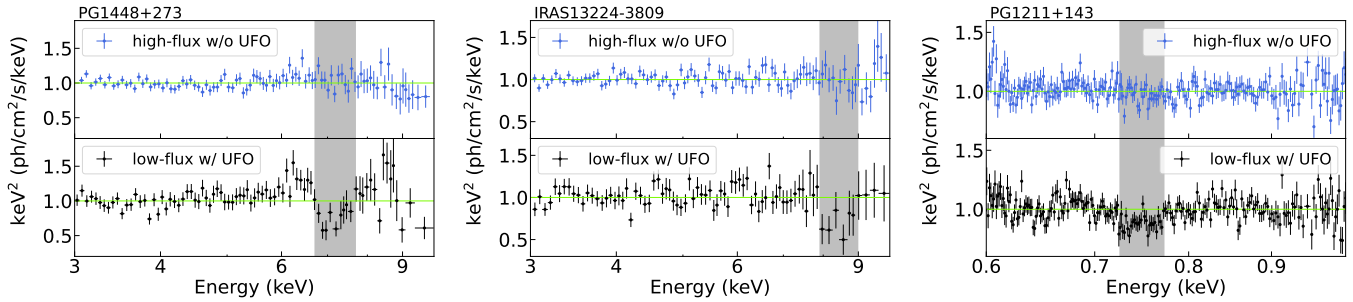

Fig. 1. Data-to-model ratios of stacked EPIC (PG 1448 and IRAS 13224) and RGS (PG 1211) spectra to the best-fit broadband continuum model (see details in Sect. 3). The "high-flux w/o UFO" and "low-flux w/ UFO" results are marked by royal blue and black points, respectively. The energy band distinctly affected by the UFO is marked by the gray region.

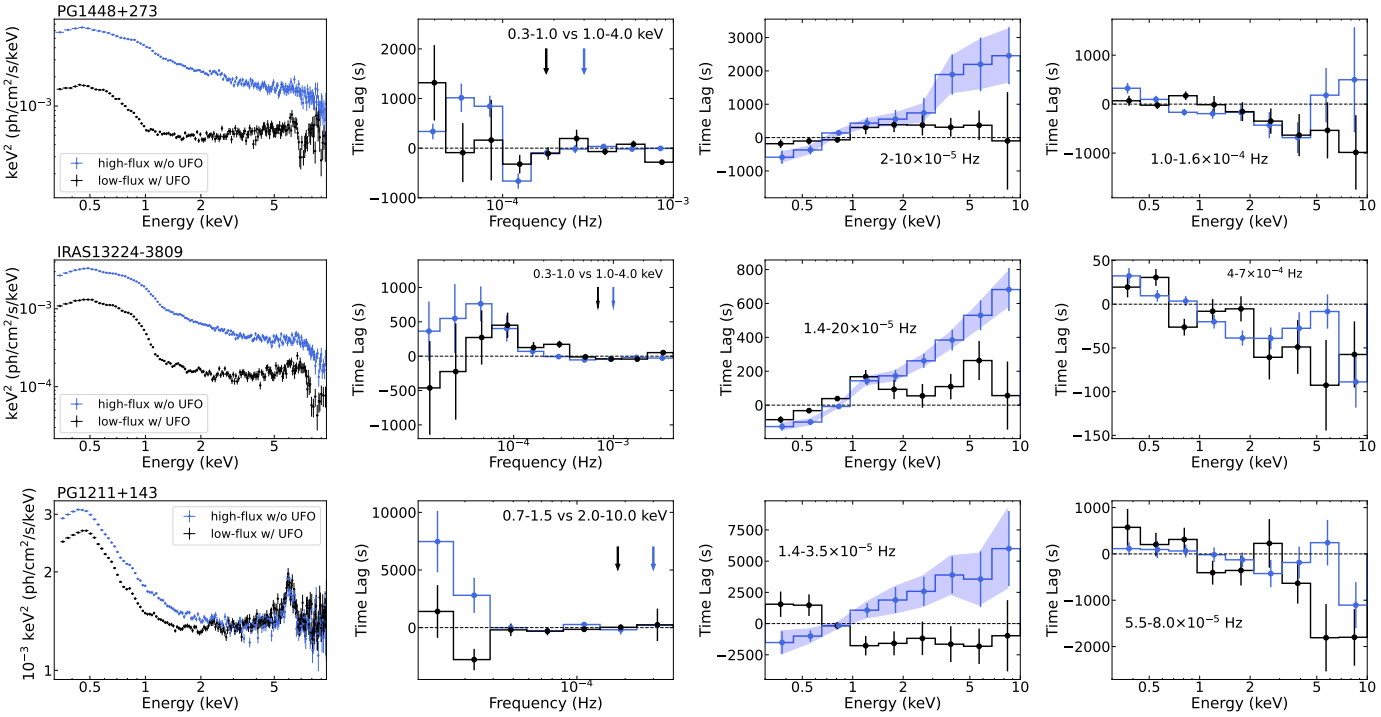

Fig. 2. X-ray time lags for PG 1448 (top), IRAS 13224 (middle), and PG 1211 (bottom). The "low-/high-flux w/wo UFO" observations are marked in black and royal blue, respectively. The first column shows the unfolded stacked flux energy spectrum with respect to a power law of $\Gamma = 2$ of each AGN. The second column shows the lag-frequency spectrum between soft and hard energy bands. The arrows separately refer to the frequencies, at which the PSD of the highest-energy bin (in the lag-energy spectra) becomes dominated by Poisson noise, for the corresponding stacked observations. The third and fourth columns present the low- (third) and high-frequency (fourth) lag-energy spectra separately at particular frequencies, marked in the plots. The shaded blue regions in the low-frequency lag-energy spectra show the 1σ spread in lags from MC simulations (see details in Sect. 3.2).

to its tiny lag amplitude (~100 s), which is aligned with the literature (e.g., Kara et al. 2013c; Alston et al. 2020). The lag-frequency spectra of "low-/high-flux w/wo UFO" observations are more or less consistent within the uncertainties. However, it generally indicates that the "high-flux w/o UFO" observations have a larger low-frequency hard lag than "low-flux w/ UFO" observations.

3.2. Lag-energy spectra

The lag-energy spectra were computed in a similar way to the lag-frequency spectrum. The only difference is that, at this moment, the lag is calculated in a particular frequency range between a narrow band of interest and a large reference band. To obtain the best S/N, we chose the reference band to be the entire 0.3–10 keV, and removed the band of interest so that the noise was not correlated. The frequency ranges for the lag-energy spectra were chosen based on the lag-frequency spectra and marked in the plots. As a conservative approach, the upper bound of the high-frequency lag-energy spectrum was set by the frequency at which the PSD of the hardest energy band becomes dominated by Poisson noise (indicated by arrows in Fig. 2).

For observations unaffected by obscuration, the lag-energy spectra present an increasing lag with energy at low frequencies and a soft excess lag plus an iron K reverberation lag at high frequencies, which is consistent with previous results for IRAS 13224 and PG 1211 (Kara et al. 2013c; Lobban et al. 2018; Hancock et al. 2022). On the other hand, this is also the first time these typical AGN X-ray time lags have been detected in PG 1448. Regarding observations obscured by UFOs, we repro-

Table 2. Significance of the deviation between low-frequency lag-energy spectra of two stacked observations in AGNs with a transient UFO.

Names	$P_{\rm null}^{\rm Cal}$	$\sigma_{\rm Cal}$	$P_{\rm null}^{\rm MC}$	$\sigma_{\rm MC}$
PG 1448+273	0.006	2.7	0.003	2.8
IRAS 13224-3809	6.6×10^{-8}	5.4	1.9×10^{-8}	5.6
PG 1211+143	3.4×10^{-7}	5.1	1.7×10^{-6}	4.7

Notes. Two kinds of null hypothesis probability, $P_{\rm null}$, and the significance σ of deviation were calculated by the χ^2 statistics of lags with uncertainties using the method in Nowak & Vaughan (1996) and the MC method, respectively. Both approaches confirm that the low-frequency lag-energy spectra in the "low-flux w/ UFO" state are different from those of the "high-flux w/o UFO" state.

duced the same results of PG 1211 discovered in Lobban et al. (2018) that the low-frequency ($1.4-3.5\times10^{-5}$ Hz) hard lag changes to flatter. Furthermore, we find that this phenomenon also appears in the other two AGNs, which is compatible with the results of lag-frequency spectra. In the high-frequency domain, the soft lags still exist, while the iron K reverberation lag seems to disappear or become weak. However, due to the smaller number of counts in the low-flux state, especially in the Fe K band, we cannot conclude that the origin of the disappearance or weakness of the Fe K reverberation lag is physical or just limited by data quality.

To quantify the significance of the deviation between the low-frequency lag-energy spectra of two states, we adopted the χ^2 statistics by assuming one spectrum as the expected values and the other as the observed values. The calculated null hypothesis probability, $P_{\rm null}^{\rm Cal}$, and corresponding significance, $\sigma_{\rm Cal}$, are shown in Table 2, where all cases exhibit a deviation significance larger than 2.7σ. The deviation is also confirmed by Monte Carlo (MC) simulations. Following the method described in Timmer & König (1995), we used the `GaussianResponse` task in `pylag` package to simulate light curve pairs based on the observed PSD in each energy bin with a time lag described by a Gaussian response function. The Gaussian response function centers on the observed lag with the width of the lag uncertainty. The shaded blue regions in Fig. 2 represent the 1σ uncertainties in lag from 1000 MC simulated light curve pairs in each energy band, which are comparable with our calculated uncertainties (Uttley et al. 2014). The null hypothesis probability, $P_{\rm null}^{\rm MC}$, and significance, $\sigma_{\rm MC}$, of deviation were then calculated based on uncertainties obtained from MC simulations (see Table 2), where the significance is at least larger than 2.8σ. Our results show that the lag-energy spectra of the "low-flux w/ UFO" observations differ remarkably from those of the "high-flux w/o UFO" observations.

4. Discussion

Through the spectral-timing analysis of archival *XMM-Newton* observations on three AGNs with transient UFOs, we find that suppression of low-frequency hard lags during low-flux UFO-affected states is not unique in PG 1211, since the other two AGNs manifest it with a transient UFO obscuration event. However, whether the suppressed continuum lags are related to UFOs is still unknown because UFOs and low-flux states commonly appear simultaneously. Perhaps the lower lag amplitude results purely from the low flux, related to the continuum variation, and X-ray time lags are flux-dependent, as was suggested by Alston et al. (2013).

4.1. Whether UFOs are causally related to suppressed low-frequency hard lags

We therefore searched for another three bright targets with large X-ray variability but without UFOs in archival *XMM-Newton* observations: Ark 564, NGC 7469, and Mrk 335. Their X-ray time properties have been well explored, and typical low-frequency hard lags and high-frequency iron K reverberation lags have been found in all of them (e.g., Kara et al. 2013a, 2016; Mastroserio et al. 2020; Lewin et al. 2022). It should also be noted that despite the absence of UFOs in these targets, slower and less ionized absorbers were discovered in all of them (Giustini et al. 2015; Longinotti et al. 2013; Khanna et al. 2016; Mehdipour et al. 2018; Grafton-Waters et al. 2020; Liu et al. 2021).

Following the same data reduction and analysis routines, we selected archival *XMM-Newton* observations of these three targets with distinct fluxes and stacked them into low-flux and high-flux subclasses. The basic information on selected observations is listed in Table B.1. The light curves in the EPIC-pn band and the corresponding PSD are shown in Fig. B.1, exhibiting frequencies above which the Poisson noise becomes dominant. The segment lengths are 50 ks for Ark 564, and 80 ks for NGC 7469 and Mrk 335, respectively. According to the literature, the origins of the flux variation among these targets are different: the variation in Ark 564 originates mainly from the variable normalization of the broadband continuum (Giustini et al. 2015); the variation in NGC 7469 results from the variable normalization of the soft excess component (Peretz et al. 2018; Middei et al. 2018); and the variation in Mrk 335 is contributed to by both the variable intrinsic continuum and ionized absorbers (Gallo et al. 2015; Komossa et al. 2020).

The stacked flux-energy, lag-frequency, and lag-energy spectra are shown in Fig. B.2. The details of the lag-frequency and high-frequency lag-energy spectra are described in Appendix B and, briefly speaking, the flux variability has a negligible influence on them. For the low-frequency lag-energy spectra, the typical hard lags that increase with energy are observed and are consistent with each other within spectra of two flux states for every AGN. The null hypothesis probability and the significance of deviation are listed in Table 3, where no case exhibits a deviation significance greater than 1.2σ. This behavior is quite different from previous results of AGNs with UFOs, suggesting that flux changes, originating from the continuum variations, do not affect the low-frequency hard lags, and the suppression of low-frequency hard lags might be linked to UFOs. We note a tentative deviation in the low-frequency lag-energy spectrum of Mrk 335, where the deviation occurs in the highest energy bin, leading to a deviation significance of $\sim1\sigma$. However, it should be noted that the absorbers in Mrk 335 have large velocities of ~5000 to 7000 km/s (Longinotti et al. 2019), making them distinct from typical warm absorbers (WAs, $v < 1000$ km/s, Laha et al. 2021) but closer to UFOs ($v > 10\,000$ km/s). They are therefore called obscuring outflows. If the hypothesis that the presence of UFOs can suppress the low-frequency hard lags is true, this weak indication may be related to the similarity between obscuring outflows in Mrk 335 and typical UFOs.

Similar fast obscuring outflows were also observed in NGC 3783 and Mrk 817 and expected from the outer disk or broad-line region. In De Marco et al. (2020), NGC 3783 shows negative low-frequency lags in obscured observations and positive

Table 3. Significance of the deviation between low-frequency lag-energy spectra of two stacked observations in AGNs without UFOs (Similar to Fig. 3).

Names	$P_{\rm null}^{\rm Cal}$	$\sigma_{\rm Cal}$	$P_{\rm null}^{\rm MC}$	$\sigma_{\rm MC}$
Ark 564	0.90	0.12	0.96	0.05
NGC 7469	0.96	0.05	0.97	0.03
Mrk 335	0.26	1.12	0.27	1.09

Notes. Both two approaches confirm that, in AGNs without UFOs, the low-frequency lag-energy spectra of the low-flux observations are consistent with those of the high-flux ones.

Table 4. Estimates of the recombination time, absorber size, and light-crossing time of UFOs in AGNs.

Names	Recombination time (s)	Absorber size (cm)	Light-crossing time (s)
PG 1448	<10	$<2\times10^{13}$	<700
IRAS 13224	<1	$<1.4\times10^{12}$	<50
PG 1211	<100	$<5\times10^{13}$	<1700

Notes. The absorber size was calculated by assuming that the transverse velocity is equal to the Keplerian velocity. The light-crossing time of absorbers was conservatively estimated by assuming a transparent absorber for hard X-ray photons. The recombination timescale was estimated by assuming the number density of $10^{10}\,{\rm cm}^{-3}$ for PG 1448 (Reeves et al. 2023), $10^{11}\,{\rm cm}^{-3}$ for IRAS 13224 (Pinto et al. 2018), and $10^{8}\,{\rm cm}^{-3}$ for PG 1211 (Reeves et al. 2018).

low-frequency lags in unobscured exposures, which is consistent with what we observed in targets with variable UFOs. In Lewin et al. (2024), Mrk 817 exhibits low-frequency hard lags up to 800s when the source is partially obscured but relatively bright compared with other heavily obscured long *XMM-Newton* observations. As an SMBH with a mass of $3.85\times10^7\,M_\odot$, the amplitude of its low-frequency lag is smaller than those at similar masses (e.g., PG 1448) and comparable with the results for IRAS 13224 ($M_{\rm BH}\sim2\times10^6\,M_\odot$), if we assume that low-frequency lags scale with SMBH masses. This indicates that obscuring outflows might have a moderate influence (between UFOs and WAs) on suppressing low-frequency hard lags, pointing toward the suppression strength being related to outflow properties (awaiting for further works).

As a result, by comparing X-ray time lags at different flux states of AGNs without UFOs, we find no evidence that the suppressed low-frequency hard lags originate from the faint continuum flux. The results of Mrk 335, combined with archival discoveries of Mrk 817 and NGC 3783, tentatively reveal that obscuring outflows with velocities close to those of UFOs might have a moderate influence on low-frequency hard lags. In fact, our discoveries are compatible with the results of NGC 4051 discovered by Alston et al. (2013), because some ionized winds in NGC 4051 are also close to UFOs with high velocities ($v>3000$ km/s, Pounds & King 2013) and the major differences between the high- and low-flux X-ray spectra come from the varying ionized winds (Pounds et al. 2004).

4.2. Explanations for varying low-frequency hard lags

Based on our results and discussions, the suppressed hard continuum lags are likely related to the emergence of fast-moving outflows, not necessarily related to the source flux, while the underlying mechanism remains unclear.

4.2.1. Scenario I: Additional lags associated with outflows

One possible interpretation is that different physical processes dominate on different timescales. Silva et al. (2016) once investigated the NGC 4051 data using a time-dependent photoionization code to estimate the influence of outflowing ionized absorbers on X-ray time lags. They found that WAs in NGC 4051 can produce low-frequency soft X-ray lags, where the delay arises from the long radiative recombination time of WAs when the plasma varies in response to the ionizing continuum. The phenomenon of low-frequency soft X-ray lags was also observed in NGC 1365 and was explained by different light-crossing timescales of hard and soft X-ray photons in WAs (Kara et al. 2015). As a result, in this scenario, low-frequency X-ray lags comprise both signals of hard X-ray continuum lags related to the accretion flow and soft X-ray lags associated with the ionized absorbers. Similar effects might also arise in our results if soft X-ray UFOs (detected in all three targets) can enhance the time lags in the soft X-ray bands, leading to a seemingly flat lag-energy spectrum.

In general, UFOs are closer to SMBHs than WAs (e.g., Laha et al. 2021), and are expected to have a higher number density. Therefore, X-ray time lags introduced by the recombination of UFOs should have shorter timescales than those of WAs, since the recombination timescale is inversely proportional to the plasma number density (Krolik & Kriss 1995). The recombination timescales of UFOs were calculated using the `rec_time` tool in the SPEX package (Kaastra et al. 1996) with assumed number densities of $n_{\rm e}=10^{10}\,{\rm cm}^{-3}$ for PG 1448 (Reeves et al. 2023), $n_{\rm e}=10^{11}\,{\rm cm}^{-3}$ for IRAS 13224, and $n_{\rm e}>10^{8}\,{\rm cm}^{-3}$ for PG 1211 (Reeves et al. 2018). All densities were estimated with the definition of the ionization parameter, $\xi=L_{\rm ion}/n_{\rm e}R^2$, where the location of the outflow, R, was constrained by the transient timescale of the UFO, Δt, and the variation in the column density, $\Delta N_{\rm H}$, reported in the literature, $R^{5/2}=(GM)^{1/2}(L_{\rm ion}\Delta t/\Delta N_{\rm H}\xi)$. Recombination timescales are listed in Table 4. Our estimations show that delays from recombination are negligible and cannot contribute to the flat lag-energy spectra in the low-frequency domain.

The other possible contributor is the delay resulting from different light-crossing timescales for soft and hard X-rays in UFOs. We estimated the light-crossing time by assuming an extreme situation: that UFOs are transparent to hard X-rays but optically thick to soft X-rays. The light-crossing time was then related to the absorber size, ΔR, which could be derived through $\Delta R=(GM/R)^{1/2}\Delta t$ by assuming that the transverse velocity is equal to the Keplerian velocity. The resulting absorber size and light-crossing time are listed in Table 4. The light-crossing times are on an order of magnitude that is comparable with observed low-frequency lags, indicating that the additional lags associated with different light-crossing timescales of photons are promising for explaining the observed phenomenon. However, we caution that those values are generally several times lower than observed lags under a conservative condition, which weakens the likelihood of this mechanism.

4.2.2. Scenario II: Inhibited disk-corona energy transfer

Another intriguing possible scenario is that the energy transfer between the disk and corona is inhibited by outflows, preventing the propagation of accretion fluctuations if low-frequency

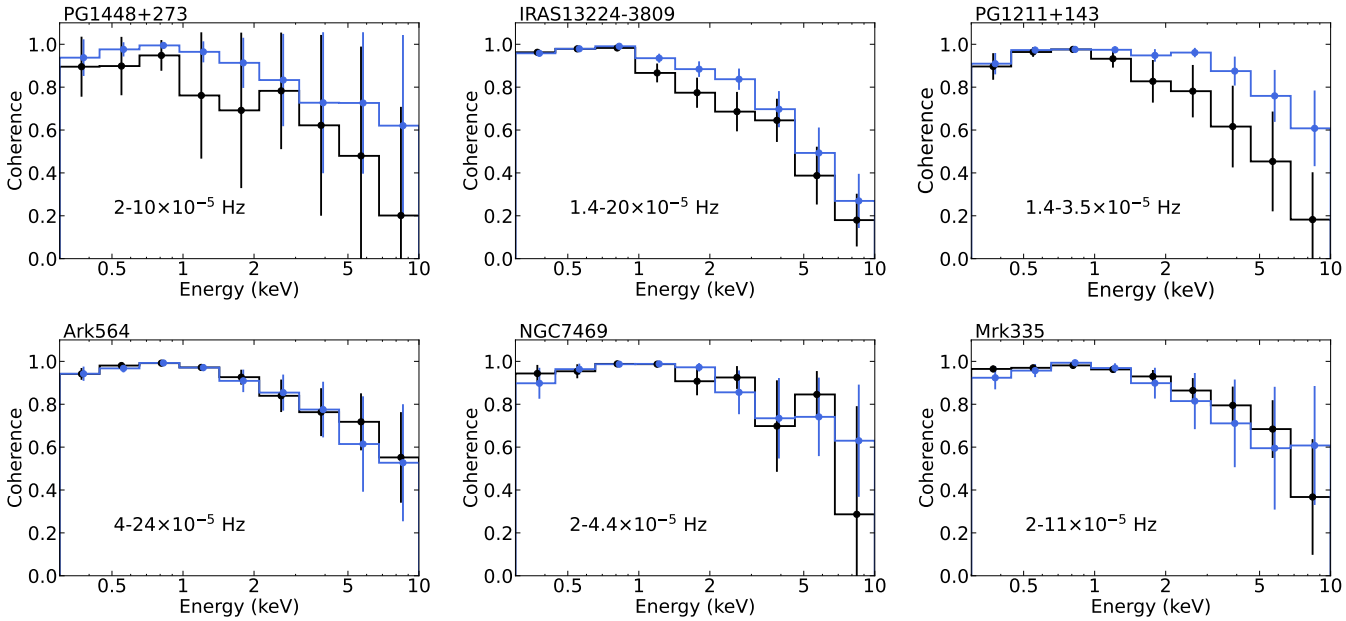

Fig. 3. Poisson noise-corrected coherence-energy spectra of UFO-(upper) or flux-resolved (lower) observations for targets analyzed in this work at low frequencies. In AGNs with transient UFOs (upper), the "low-flux w/ UFO" (black) coherence spectra are in general lower than the "high-flux w/o UFO" coherence spectra (royal blue), while the coherence spectra remain unchanged at different flux levels for AGNs without UFOs (lower).

hard lags originate from the inward-propagating mass accretion fluctuation generated in large radii (e.g., Uttley & Malzac 2024). Since UFOs, with their extreme velocities, are expected to originate from the inner accretion disk, their launching can carry away a portion of the inflowing materials from the inner disk. In this scenario, the reduction in lags results from the removal of the UV seed photons carrying fluctuations and/or the obscuration of seed photons by UFOs, leading to fewer fluctuation signals propagating into the hot corona. This explanation is supported by the differences between UFO-resolved coherence spectra at low frequencies, where the band choices are the same as those in Figs. 2 and B.2, shown in Fig. 3. In AGNs with transient UFOs (i.e., upper panels in Fig. 3), the entire coherence spectra of UFO-obscured observations are tentatively weaker than those without UFOs, although the results of PG 1448 are compatible within uncertainties due to limited exposures, while in AGNs without UFOs (lower panels), the coherence spectra at different fluxes remain consistent. These results suggest that UFOs can prevent the energy transportation between the disk and the hot corona, reducing time lags.

In this scenario, X-ray lags in the high-frequency domain are also expected to be affected by UFOs because coronal X-ray emission is correlated with mass accretion (e.g., Lusso et al. 2010; Svoboda et al. 2017). The reduction in accretion mass by outflows would decrease the coronal X-ray emission, leading to weaker signals of X-ray reprocessing in the accretion disk. Our results seem to agree with this expectation, that in AGNs with UFOs the Fe K reverberation lags of absorbed observations are less significant than those in unobscured states (see Fig. 2), while they remain almost unchanged in AGNs without UFOs (see Fig. B.2). However, it is still unclear whether their disappearance is physically related to UFOs or depends on chosen frequency bands or specific observations, and the soft lags remain constant. In addition, it is still possible that the Fe K reverberation lags occur in absorbed states if the coronal variability, in some cases, has not started to be affected by the removal of propagating fluctuations generated in larger radii.

However, supporting this hypothesis requires a dedicated theoretical simulation, incorporating accretion flows with mass fluctuation propagation and outflows launched from the inner accretion disk. This work has not been accomplished yet and should be done in the future for comparison with observational results.

5. Conclusions

Working on archival *XMM-Newton* data, we have performed a UFO-resolved spectral-timing analysis of three AGNs with transient UFOs to investigate the potential influence of UFOs on X-ray time lags. As a result, we have shown that low-frequency hard lags become weak, accompanied by UFOs, in all three targets. Our investigations of another three variable AGNs without UFOs indicate that suppressed low-frequency hard lags might be unrelated to flux variability. Results of Mrk 335 with fast-moving obscuring outflows, combined with archival results in Mrk 817 and NGC 3783, even indicate an intermediate state of effects between UFOs and slow WAs. We propose an additional time delay associated with UFOs or the inhibited energy and variability transfer between the disk and corona for explanations. Our work indicates that any analysis of X-ray time lags in AGNs must account for the potential effects of ionized absorbers if they are present. The same investigation like this work should be extended to more sources, particularly with various black hole masses and accretion rates, to justify proposed explanations.

Acknowledgements. The authors thank Phil Uttley, Matteo Lucchini, Peter Kosec, and the anonymous referee for constructive suggestions. This research has made use of data obtained with the *XMM-Newton*, an ESA science mission funded by ESA Member States and the USA (NASA). YX, CP, and SB acknowledge support for PRIN MUR 2022 SEAWIND 2022Y2T94C (funded by NextGenerationEU) and INAF LG 2023 BLOSSOM. EK acknowledges the XRISM Participating Scientist Program for support under NASA grant 80NSSC20K0733. FT acknowledges funding from the European Union - Next Generation EU, PRIN/MUR 2022 (2022K9N5B4).

References

Allen, D. A., Norris, R. P., Meadows, V. S., & Roche, P. F. 1991, MNRAS, 248, 528
Alston, W. N., Vaughan, S., & Uttley, P. 2013, MNRAS, 435, 1511
Alston, W. N., Fabian, A. C., Kara, E., et al. 2020, Nat. Astron., 4, 597
Arévalo, P., & Uttley, P. 2006, MNRAS, 367, 801
Ballantyne, D. R., Sudhakar, V., Fairfax, D., et al. 2024, MNRAS, 530, 1603
Bartlett, M. S. 1948, Nature, 161, 686
Belloni, T., & Hasinger, G. 1990, A&A, 227, L33
Chartas, G., Brandt, W. N., Gallagher, S. C., & Garmire, G. P. 2002, ApJ, 579, 169
Chartas, G., Brandt, W. N., & Gallagher, S. C. 2003, ApJ, 595, 85
Chartas, G., Cappi, M., Vignali, C., et al. 2021, ApJ, 920, 24
Danehkar, A., Nowak, M. A., Lee, J. C., et al. 2018, ApJ, 853, 165
De Marco, B., Ponti, G., Cappi, M., et al. 2013, MNRAS, 431, 2441
De Marco, B., Adhikari, T. P., Ponti, G., et al. 2020, A&A, 634, A65
Di Matteo, T., Springel, V., & Hernquist, L. 2005, Nature, 433, 604
Done, C., Davis, S. W., Jin, C., Blaes, O., & Ward, M. 2012, MNRAS, 420, 1848
Fabian, A. C. 2012, ARA&A, 50, 455
Fabian, A. C., Rees, M. J., Stella, L., & White, N. E. 1989, MNRAS, 238, 729
Fabian, A. C., Zoghbi, A., Ross, R. R., et al. 2009, Nature, 459, 540
Gallo, L. C., Wilkins, D. R., Bonson, K., et al. 2015, MNRAS, 446, 633
García, J., & Kallman, T. R. 2010, ApJ, 718, 695
García, J. A., Kara, E., Walton, D., et al. 2019, ApJ, 871, 88
George, I. M., & Fabian, A. C. 1991, MNRAS, 249, 352
Giustini, M., Turner, T. J., Reeves, J. N., et al. 2015, A&A, 577, A8
Gofford, J., Reeves, J. N., Tombesi, F., et al. 2013, MNRAS, 430, 60
Grafton-Waters, S., Branduardi-Raymont, G., Mehdipour, M., et al. 2020, A&A, 633, A62
Haardt, F., & Maraschi, L. 1993, ApJ, 413, 507
Hancock, S., Young, A. J., & Chainakun, P. 2022, MNRAS, 514, 5403
Härer, L., Parker, M. L., Joyce, A., et al. 2021, MNRAS, 500, 4506
Hopkins, P. F., & Elvis, M. 2010, MNRAS, 401, 7
Igo, Z., Parker, M. L., Matzeu, G. A., et al. 2020, MNRAS, 493, 1088
Jansen, F., Lumb, D., Altieri, B., et al. 2001, A&A, 365, L1
Kaastra, J. S., Mewe, R., & Nieuwenhuijzen, H. 1996, in UV and X-ray Spectroscopy of Astrophysical and Laboratory Plasmas, 411
Kara, E., Fabian, A. C., Cackett, E. M., et al. 2013a, MNRAS, 434, 1129
Kara, E., Fabian, A. C., Cackett, E. M., et al. 2013b, MNRAS, 428, 2795
Kara, E., Fabian, A. C., Cackett, E. M., Miniutti, G., & Uttley, P. 2013c, MNRAS, 430, 1408
Kara, E., Zoghbi, A., Marinucci, A., et al. 2015, MNRAS, 446, 737
Kara, E., Alston, W. N., Fabian, A. C., et al. 2016, MNRAS, 462, 511
Khanna, S., Kaastra, J. S., & Mehdipour, M. 2016, A&A, 586, A2
Komossa, S., Grupe, D., Gallo, L. C., et al. 2020, A&A, 643, L7
Kosec, P., Zoghbi, A., Walton, D. J., et al. 2020, MNRAS, 495, 4769
Kotov, O., Churazov, E., & Gilfanov, M. 2001, MNRAS, 327, 799
Kriss, G. A., Lee, J. C., Danehkar, A., et al. 2018, ApJ, 853, 166
Krolik, J. H., & Begelman, M. C. 1988, ApJ, 329, 702
Krolik, J. H., & Kriss, G. A. 1995, ApJ, 447, 512
Laha, S., Reynolds, C. S., Reeves, J., et al. 2021, Nat. Astron., 5, 13
Laurenti, M., Luminari, A., Tombesi, F., et al. 2021, A&A, 645, A118
Lewin, C., Kara, E., Wilkins, D., et al. 2022, ApJ, 939, 109
Lewin, C., Kara, E., Barth, A. J., et al. 2024, ApJ, 974, 271
Liu, H., Parker, M. L., Jiang, J., et al. 2021, MNRAS, 506, 5190
Lobban, A. P., Vaughan, S., Pounds, K., & Reeves, J. N. 2016, MNRAS, 457, 38
Lobban, A. P., Vaughan, S., Pounds, K., & Reeves, J. N. 2018, MNRAS, 476, 225
Longinotti, A. L., Krongold, Y., Kriss, G. A., et al. 2013, ApJ, 766, 104
Longinotti, A. L., Kriss, G., Krongold, Y., et al. 2019, ApJ, 875, 150
Lusso, E., Comastri, A., Vignali, C., et al. 2010, A&A, 512, A34
Lyubarskii, Y. E. 1997, MNRAS, 292, 679
Marziani, P., Sulentic, J. W., Dultzin-Hacyan, D., Calvani, M., & Moles, M. 1996, ApJS, 104, 37
Mastroserio, G., Ingram, A., & van der Klis, M. 2020, MNRAS, 498, 4971
Matzeu, G. A., Brusa, M., Lanzuisi, G., et al. 2023, A&A, 670, A182
Mehdipour, M., Kaastra, J. S., Costantini, E., et al. 2018, A&A, 615, A72
Middei, R., Bianchi, S., Cappi, M., et al. 2018, A&A, 615, A163
Mizumoto, M., Done, C., Hagino, K., et al. 2018, MNRAS, 478, 971
Mizumoto, M., Ebisawa, K., Tsujimoto, M., et al. 2019, MNRAS, 482, 5316
Netzer, H. 2013, The Physics and Evolution of Active Galactic Nuclei (Cambridge, UK: Cambridge University Press)
Nowak, M. A., & Vaughan, B. A. 1996, MNRAS, 280, 227
Papadakis, I. E., Nandra, K., & Kazanas, D. 2001, ApJ, 554, L133
Parker, M. L., Alston, W. N., Buisson, D. J. K., et al. 2017a, MNRAS, 469, 1553
Parker, M. L., Pinto, C., Fabian, A. C., et al. 2017b, Nature, 543, 83
Parker, M. L., Reeves, J. N., Matzeu, G. A., Buisson, D. J. K., & Fabian, A. C. 2018, MNRAS, 474, 108
Parker, M. L., Alston, W. N., Härer, L., et al. 2021, MNRAS, 508, 1798
Patrick, A. R., Reeves, J. N., Porquet, D., et al. 2012, MNRAS, 426, 2522
Peretz, U., Behar, E., Kriss, G. A., et al. 2018, A&A, 609, A35
Peterson, B. M., Ferrarese, L., Gilbert, K. M., et al. 2004, ApJ, 613, 682
Petrucci, P. O., Ursini, F., De Rosa, A., et al. 2018, A&A, 611, A59
Petrucci, P. O., Gronkiewicz, D., Rozanska, A., et al. 2020, A&A, 634, A85
Pinto, C., Alston, W., Parker, M. L., et al. 2018, MNRAS, 476, 1021
Ponti, G., Gallo, L. C., Fabian, A. C., et al. 2010, MNRAS, 406, 2591
Ponti, G., Papadakis, I., Bianchi, S., et al. 2012, A&A, 542, A83
Porquet, D., Reeves, J. N., Matt, G., et al. 2018, A&A, 609, A42
Porquet, D., Reeves, J. N., Grosso, N., Braito, V., & Lobban, A. 2021, A&A, 654, A89
Pounds, K. A., & King, A. R. 2013, MNRAS, 433, 1369
Pounds, K., & Nayakshin, S. 2023, MNRAS, submitted [arXiv:2310.18105]
Pounds, K. A., & Reeves, J. N. 2009, MNRAS, 397, 249
Pounds, K. A., King, A. R., Page, K. L., & O'Brien, P. T. 2003, MNRAS, 346, 1025
Pounds, K. A., Reeves, J. N., King, A. R., & Page, K. L. 2004, MNRAS, 350, 10
Pounds, K. A., Lobban, A., Reeves, J. N., Vaughan, S., & Costa, M. 2016a, MNRAS, 459, 4389
Pounds, K., Lobban, A., Reeves, J., & Vaughan, S. 2016b, MNRAS, 457, 2951
Rakshit, S., Stalin, C. S., & Kotilainen, J. 2020, ApJS, 249, 17
Reeves, J. N., Lobban, A., & Pounds, K. A. 2018, ApJ, 854, 28
Reeves, J. N., Braito, V., Porquet, D., et al. 2023, ApJ, 952, 52
Ross, R. R., & Fabian, A. C. 2005, MNRAS, 358, 211
Shakura, N. I., & Sunyaev, R. A. 1973, A&A, 24, 337
Silva, C. V., Uttley, P., & Costantini, E. 2016, A&A, 596, A79
Strüder, L., Briel, U., Dennerl, K., et al. 2001, A&A, 365, L18
Sunyaev, R. A., & Titarchuk, L. G. 1980, A&A, 86, 121
Svoboda, J., Guainazzi, M., & Merloni, A. 2017, A&A, 603, A127
Timmer, J., & König, M. 1995, A&A, 300, 707
Tombesi, F., Cappi, M., Reeves, J. N., et al. 2010, A&A, 521, A57
Tombesi, F., Cappi, M., Reeves, J. N., et al. 2013, MNRAS, 430, 1102
Uttley, P., & Malzac, J. 2024, MNRAS, submitted [arXiv:2312.08302]
Uttley, P., Cackett, E. M., Fabian, A. C., Kara, E., & Wilkins, D. R. 2014, A&ARv, 22, 72
van der Klis, M. 1989, in NATO Advanced Study Institute (ASI) Series C, eds. H. Ögelman, & E. P. J. van den Heuvel, Timing Neutron Stars, 262, 27
Vestergaard, M., & Peterson, B. M. 2006, ApJ, 641, 689
Wilkins, D. R. 2019, MNRAS, 489, 1957
Xiang, X., Ballantyne, D. R., Bianchi, S., et al. 2022, MNRAS, 515, 353
Xu, Y., García, J. A., Walton, D. J., et al. 2021, ApJ, 913, 13
Xu, Y., Pinto, C., Rogantini, D., et al. 2024, A&A, 687, A179
Yamada, S., Kawamuro, T., Mizumoto, M., et al. 2024, ApJS, 274, 8
Zhou, X.-L., & Wang, J.-M. 2005, ApJ, 618, L83
Zoghbi, A., Fabian, A. C., Uttley, P., et al. 2010, MNRAS, 401, 2419

Appendix A: Supplementary results of AGN with a transient UFO

The background-subtracted light curves are extracted by the package EPICLCCORR and are shown in the top panels of Fig. A.1. Observations are classified as the "low-flux w/ UFO" and "high-flux w/o UFO" states, marked in black and royal blue respectively.

For each AGN with UFOs, the stacked PSD spectra of each classification (in 0.3–10 keV energy band) were computed by the `pylag` package Bartlett 1948; van der Klis 1989; Uttley et al. 2014) and were normalized to units of fractional variance per hertz (Belloni & Hasinger 1990). The minimum frequency is defined by the inverse of the length of the observation (though we did not include the lowest-frequency bin as this is often biased by red noise leakage), and the maximum frequency is set by the frequency at which the PSD becomes dominated by Poisson noise. We binned the PSD in equal logarithmic frequency bins, and the number of frequency bins depends on the quality of the data (i.e., more bins for higher-quality data). The computed PSD functions of each AGN are shown in the bottom panels of Fig. A.1. Here, the Y-axis is in units of frequency*periodogram to illustrate the region dominated by Poisson noise, where the quantity of the Y-axis increases with frequency.

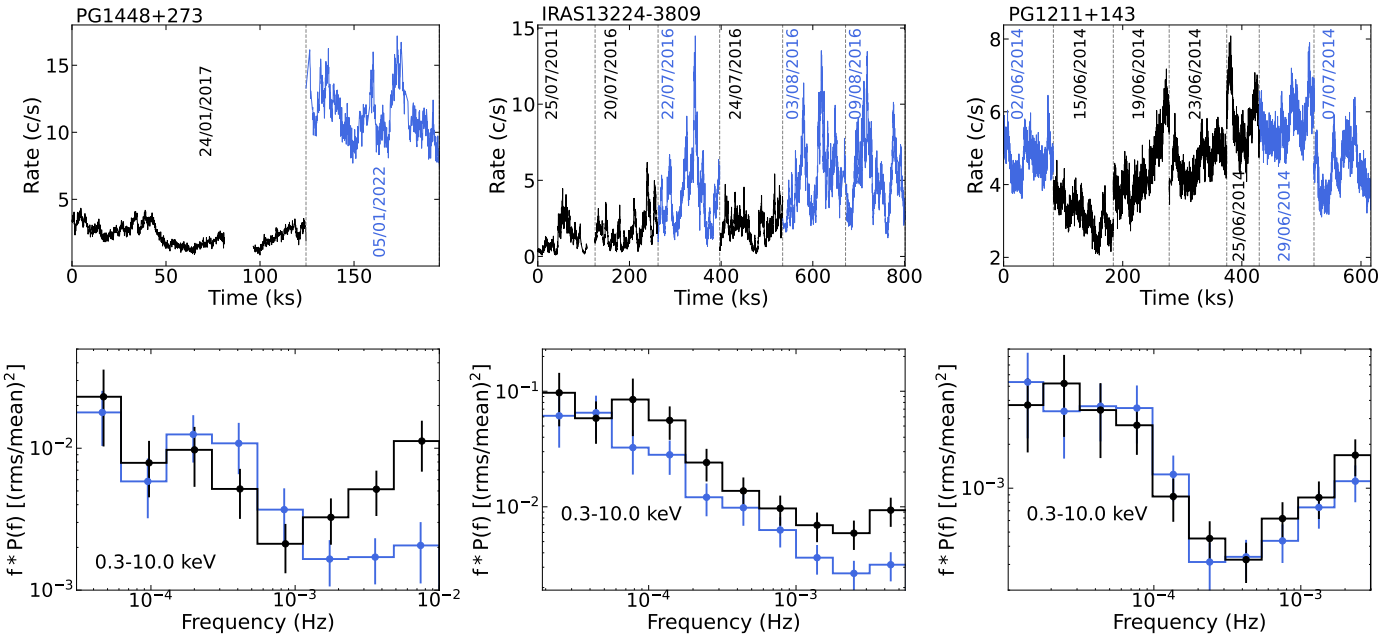

Fig. A.1. EPIC-pn (0.3–10 *keV*) light curves (top) and PSD (bottom) of PG 1448 (left), IRAS 13224 (middle), and PG 1211 (right). The "low-/high-flux w/wo UFO" observations are marked by the black and royal blue, respectively.

Appendix B: Supplementary results of targets without a transient UFO

The basic information on the selected AGN observations without transient UFOs is listed in Table 3, including the observation classification, observation IDs, net EPIC-pn exposure time, and the corresponding count rates. Observations in each AGN are classified as 'low-flux' and 'high-flux' states for the investigation discussed in Sect. 4.1 that whether the varying low-frequency hard lags are related to the source luminosity.

Table B.1. *XMM-Newton* observations of the three AGN without a transient UFO mentioned in Sect. 4.

Source	Label	Obs. ID	Exposure (ks)	Count Rates (cts/s)
Ark 564	Low-flux	0206400101, 0670130701, 0830540101	69, 36, 79	37.9, 29.5, 31.4
	High-flux	0670130201, 0670130501, 0670130901	41, 47, 39	61.8, 49.7, 57.1
NGC 7469	Low-flux	0760350401, 0760350501	52, 60.0	18.7, 19.7
	High-flux	0207090101, 0760350201	59, 61	25.2, 26.1
Mrk 335	Low-flux	0600540601, 0600540501⋆, 0842761301⋆, 0842760201, 0842761101	97, 69, 76, 74, 74	3.1, 4.3, 5.3, 3.2, 3.6
	High-flux	0306870101	92	26.3

⋆ The source spectrum is extracted from an annulus region with an inner radius of 5 arcsec and an outer radius of 30 arcsec. **Notes.** Similar to Table 1. The second column shows the label for stacked observations at two states. The observation IDs are shown in the third column. The corresponding net exposure time and count rate of EPIC-pn are listed in the fourth and fifth columns, respectively.

The background-subtracted light curves of AGN without transient UFOs and corresponding periodogram are shown in Fig. B.1, similar to Fig. A.1. The frequencies at which the Poisson noise becomes dominant can be obtained from our PSD spectra.

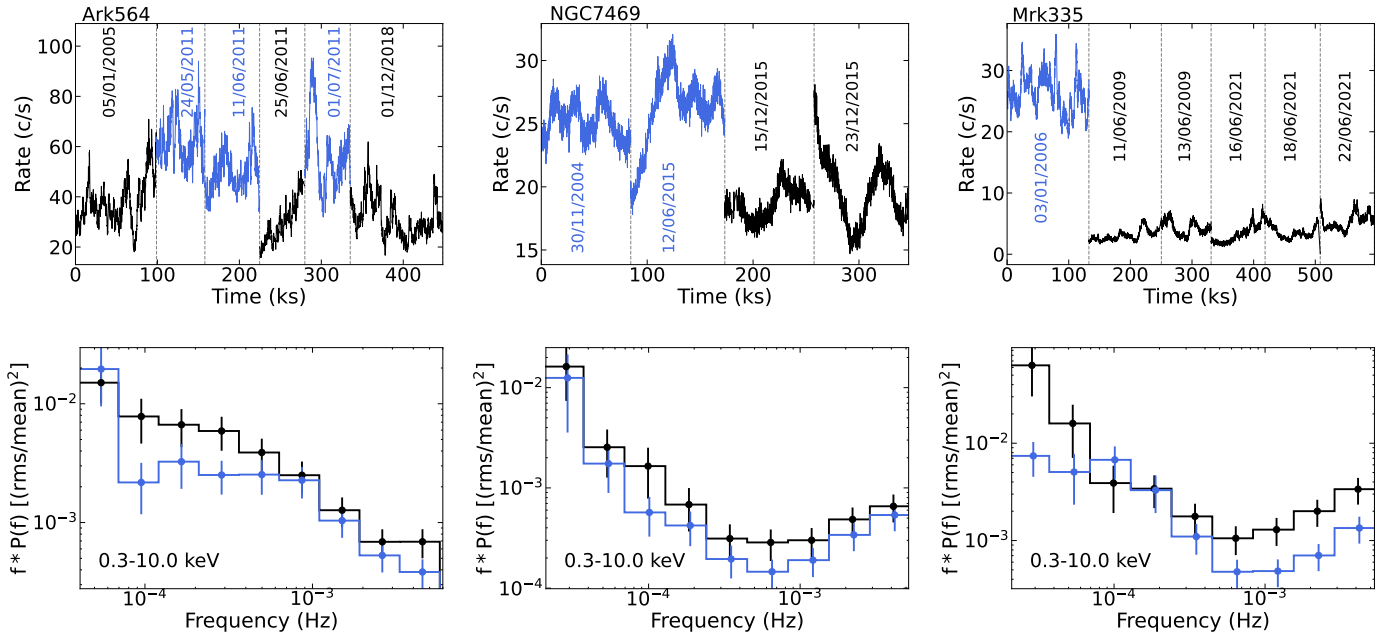

Fig. B.1. EPIC-pn light curves (top) and PSD (bottom) of Ark 564 (left), NGC 7469 (middle), and Mrk 335 (right). The "low-/high-flux" observations are marked in black and royal blue, respectively.

For each AGN, the stacked flux energy spectra of observations at different flux states are shown in the first column of Fig. B.2. The spectral variations are different among these AGN. The spectral variation of Ark 564 appears in the entire EPIC band without significant changes in the spectral slope, while that of NGC 7469 only occurs in the soft X-ray band, revealing that the soft excess mainly contributes to its spectral and flux variations. In Mrk 335, changes take place in both the spectral slope and spectral normalization, indicating that the variability originates from both broadband continuum variations and ionized absorbers (Gallo et al. 2015; Komossa et al. 2020).

The stacked flux-energy, lag-frequency, and lag-energy spectra are shown in Fig. B.2, while the low-frequency lag-energy spectra are discussed in detail in Sect. 3.2. The lag-frequency spectra of stacked observations at different flux states are generally consistent within uncertainties, with the exception that lags of NGC 7469 flip in the 4.4–10 $\times$ 10^{-5} Hz band, illustrated in its high-frequency lag-energy spectrum. In the high-frequency lag-energy spectra, the Fe K reverberation lag occurs in most cases regardless of the brightness, except for the high-flux state of Ark 564. We emphasize that the lags in Fig. B.2 are the stacked results, and the disappeared Fe K lags do not mean Ark 564 is special since some Fe K reverberation results are from specific observations, and not from all available observations (Kara et al. 2016). For example, when we calculate the lag-energy spectra within the same frequency band for individual high-flux observations, the Fe K lag only occurs in the observation performed on 01/07/2011, and it thus disappears in the averaged lags. The lags in the soft X-ray band are consistent with the lag-frequency spectra, where soft X-ray lags appear in nearly all spectra except for the high-flux spectrum of NGC 7469, the origin of which is beyond the scope of this work.

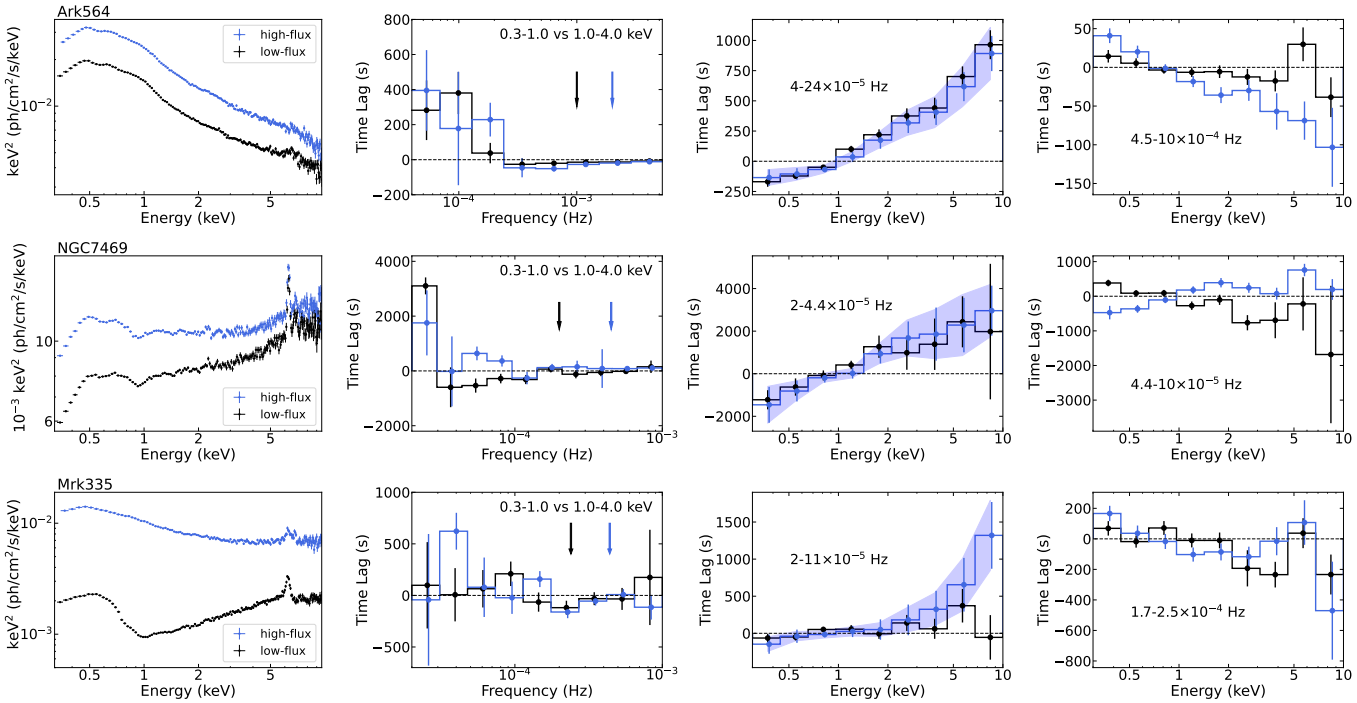

Fig. B.2. X-ray time lags for Ark 564 (top), NGC 7469 (middle), and Mrk 335 (bottom).